

We are IntechOpen, the world's leading publisher of Open Access books Built by scientists, for scientists

6,900

Open access books available

186,000

International authors and editors

200M

Downloads

Our authors are among the

154

Countries delivered to

TOP 1%

most cited scientists

12.2%

Contributors from top 500 universities



WEB OF SCIENCE™

Selection of our books indexed in the Book Citation Index
in Web of Science™ Core Collection (BKCI)

Interested in publishing with us?
Contact book.department@intechopen.com

Numbers displayed above are based on latest data collected.
For more information visit www.intechopen.com



Effective Medium Theories and Symmetry Properties of Elastic Metamaterials

Ying Wu¹, Yun Lai² and Zhao-Qing Zhang³

¹*Division of Mathematical and Computer Sciences and Engineering,
King Abdullah University of Science and Technology*

²*Department of Physics, Soochow University*

³*Department of Physics and William Mong Institute of Nano Science and Technology
Hong Kong University of Science and Technology*

¹*Saudi Arabia*

^{2,3}*China*

1. Introduction

Recently, metamaterials have attracted a great deal of attention due to their unusual properties not seen in naturally occurring materials, such as negative refraction (Lezec et al., 2007; Pendry, 2000; Veselago, 1968), superlensing (Grbic & Eleftheriades, 2004) and cloaking (Leonhardt 2006; Pendry et al., 2006), etc. These unusual properties are derived from the resonant structures in their artificial building blocks. The resonant structures interact with the wave, but their small size prevents them from being “seen” individually by the wave with wavelength inside the background much larger than the size of the structures (Pendry & Smith, 2006). Thus, the properties of a metamaterial can be described with homogenized parameters or effective medium parameters. The theory that links the microscopic resonant structures to their effective medium parameters is called the effective medium theory (EMT). For example, the left-handed metamaterial consisting of a periodic array of split ring resonators and conducting thin wires has been successfully demonstrated that, in a frequency regime, it behaves like a homogeneous medium exhibiting negative effective permittivity, ϵ_{eff} , and negative effective permeability, μ_{eff} , simultaneously (Pendry et al., 1999, 1996). Since the refractive index is defined as $n_{eff} = \sqrt{\epsilon_{eff} \mu_{eff}}$, negative refraction is a consequence of double negativity in permittivity and permeability. This example shows how effective medium parameters of particular resonant structures can be used to describe unusual properties of a metamaterial. In turn, a valid and accurate EMT provides an efficient and systematic tool to design and engineer the resonant structures according to certain desired metamaterial properties. During the development of metamaterials, there has always been a continuous effort to find an appropriate EMT for metamaterials such that various novel phenomena can have a theoretical explanation. One can obtain the effective parameters from some phenomenological results, such as transmission and reflections (Baker-Jarvis et al., 1990; Smith et al., 2002), and wave propagation (Andryieuski et al., 2009), but only a theory can give a clear understanding on the physical origin of effective

parameters. Therefore, EMTs with physical insights can be regarded as theoretical foundations of metamaterials.

The development of EMT has seen a long history accompanied by various approaches. A famous one for electromagnetic (EM) waves is the Maxwell-Garnett theory (Sheng, 2006), which is valid in the quasi-static limit, aka the zero frequency limit. The quasi-static limit requires the wavelengths inside the scatterer, the host, and the effective medium to all be very large compared to the size of the building block (Lamb et al., 1980). However, for metamaterials, the wavelength inside the scatterer could be smaller than the size of the building block and thus lead to resonances at low frequencies. This results in the failure of the widely used quasi-static EMT. Nevertheless, as long as the wavelength in the effective medium is still large compared to the size of the building block, there exists an effective medium description as the wave still cannot probe the fine structures of the building blocks. In this context, another limit is introduced, which is the long wavelength limit. Compared with the quasi-static limit, the long wavelength limit does not have restrictions on the wavelength inside the scatterer, while the wavelengths inside the host and the effective medium should still be large (Lamb et al., 1980). In the study of metamaterials, one aspect is to develop EMTs that are valid in the long wavelength limit. In this chapter, we will focus on the recent developments of EMTs for elastic metamaterials.

1.1 Effective medium theories for electromagnetic metamaterials

Though our focus is on elastic metamaterials, it is necessary to briefly review the EMTs for EM metamaterials to offer a systematic picture of the EMTs. Ever since the birth of EM metamaterials, EMTs have played an integral role in designing metamaterials and explaining their unusual properties. The EMTs for EM metamaterials can be broken down into one of several classes. In one class, the effective parameters are obtained from the average of the computed eigenfields in the unit cell (Chern & Chen, 2009; Chui & L. Hu, 2002; Pendry et al., 1999; Smith & Pendry, 2006). This method gives inherently nonlocal parameters, i.e. parameters that depend on not only frequency but also the Bloch wave vector. For metamaterials with a good effective medium approximation, the nonlocality may be ignored. This method is especially helpful for use with metamaterials with complicated unit structures, such as split rings. Another class of EMTs is called the coherent potential approximation (CPA) method. In this method the effective medium is taken as the background embedded with the scatterer in the unit cell and by implying zero scattering, some elegant formulas of the effective parameters have been obtained (X. Hu et al., 2006; Jin et al., 2009; Wu et al., 2006). This method currently only works for scatterers with isotropic geometry, but it is very accurate in the long wavelength limit even at relatively high frequencies. Interestingly, the obtained effective parameters do not have any imaginary parts if the system does not have any absorption. Similar formulas can also be obtained from the multiple-scattering theory (MST) (Chui & Lin, 2008; Wu & Z. Zhang, 2009). The MST, which will be introduced in Section 2, is capable of producing the dispersion relations of a periodic structure. From dispersion relations, the effective wave speed can be easily calculated while the impedance still remains unknown. Recently, other methods have appeared, such as the quasimode method (Sun et al., 2009) and the first-principles method (Andrea, 2011).

1.2 Effective medium theories for acoustic metamaterials

While the field of EM metamaterial has developed rapidly during the past decade, one of its counterparts, denoted as acoustic metamaterial has also seen fast growth (Ding et al., 2007; Fang et al., 2006; Lee et al., 2010; Yang et al., 2008). The acoustic metamaterial is designed to manipulate acoustic waves (Chen et al., 2010; Lu et al., 2009). Analogous to EM metamaterials, there are two material parameters that describe the wave propagation, which are bulk modulus, κ , and mass density, ρ . In two dimensions (2D), if the constituents of the metamaterials are all fluids, the governing equation can be mapped into 2D EM equations so that the EMT for 2D acoustic metamaterials is the same as that for 2D EM metamaterials. If the scatterers in acoustic metamaterials are solid, the shear modulus of the scatterers can be ignored when the longitudinal velocity contrast between the scatterer and the host is high (Kafesaki & Economou, 1999). In this case, the scattering property is basically the same as the EM cases. The mapping from the EM waves to acoustic waves facilitates the development of EMTs which have also been extensively studied by using various types of methods. MST (Mei et al., 2006; Torrent et al., 2006) and the CPA (Kafesaki et al., 2000; Li & Chan, 2004) represent two classes of them. Exciting news also came from the experimental realizations of acoustic metamaterials, such as acoustic negative refraction (S. Zhang et al., 2009) and acoustic cloaking (S. Zhang et al., 2011).

1.3 Effective medium theories for elastic metamaterials

The term *elastic* metamaterial refers to those metamaterials which are able to sustain not only longitudinal but also shear waves in their effective media. It is well-known that the EMT for an elastic composite in the quasi-static limit is anisotropic in general. The only exception is the hexagonal lattice in two dimensions (Landau & Lifshitz, 1986; Royer & Dieulesaint, 1999; Wu & Z. Zhang 2009). Even for this case, the EMT involves the determination of three effective parameters, i.e., mass density, ρ , bulk modulus, κ , and shear modulus, μ . This is in contrast to the cases of previously mentioned EM and acoustic EMTs which involve only two effective parameters. One more effective medium parameter greatly enriches the types and physics of wave propagation (Chen et al., 2008; Wu et al., 2007), such as mode conversion between longitudinal and transverse waves (Wu et al., 2011); however, it also adds complexity to the EMT. Recently, various EMTs for elastic metamaterials have been proposed, such as those ones based on the plane-wave-expansion method (Krokhin et al., 2003), and integration of fields (Zhou & Hu, 2009).

In this chapter, the symmetry property of an elastic metamaterial is examined based on the MST. It is shown that the elastic metamaterial preserves the quasi-static symmetry properties. For isotropic elastic metamaterials, CPA provides a simple and accurate EMT in the long wavelength limit, which links the scattering properties of the scatterer and the effective medium parameters (Wu et al, 2007). Those formulae can also be derived by using the MST method (Wu & Z. Zhang, 2009). For anisotropic elastic metamaterial, the EMT involves three or more effective elastic moduli (Landau & Lifshitz, 1986). In this case, CPA fails. To tackle this problem, a method based on MST in conjunction with the Christoffel's equation (Royer & Dieulesaint, 1999) has been proposed and the expressions for effective elastic moduli have been obtained (Wu & Z. Zhang, 2009). The combinations of anisotropy

and negativities in various effective moduli can give rise to many types of novel wave propagation behaviors that are unseen in normal solids (Lai et al., 2011).

Within the scope of this chapter, all the EMTs mentioned above are limited to linear elastodynamics and do not consider the micro-structure introduced local rotation (Milton & Willis, 2007).

2. Scattering properties of elastic metamaterials

In order to illustrate EMTs and symmetry properties of elastic metamaterials, we start with a simple case where the resonant scatterer in a building block is homogeneous. More complicated scatterers will be discussed in Section 5. The elastic metamaterial considered here is composed of cylindrical inclusions of radius r_s with mass density ρ_s , shear modulus μ_s , and bulk modulus κ_s , embedded in an isotropic matrix, whose material parameters are denoted by $(\rho_0, \mu_0, \kappa_0)$. In two dimensions, the bulk modulus, κ , is related to the shear modulus through the relation $\kappa = \lambda + \mu$, where λ represents the Lamé constant (Royer & Dieulesaint, 1999). Due to the translational symmetry along the cylinder's axis, denoted as z -axis, the elastic modes in the system can be decoupled into a scalar part, which is also called shear horizontal mode with vibrations along the z -axis, and a vector part, i.e., xy -mode with vibrations in the x - y plane. xy -mode is a mixed polarization of quasi-longitudinal and quasi-shear vertical modes. Since the shear horizontal mode satisfies the scalar wave equation with the same mathematical structure as those for acoustic (Krokhin et al., 2003) and 2D EM cases, this part is skipped. Rather, the focus is on the more complicated case of the xy -mode whose wave equation is given by:

$$\rho(\vec{r}) \frac{\partial^2 u_i(\vec{r})}{\partial t^2} = \nabla \cdot (\mu(\vec{r}) \nabla u_i(\vec{r})) + \nabla \cdot \left(\mu(\vec{r}) \frac{\partial \bar{u}(\vec{r})}{\partial x_i} \right) + \frac{\partial}{\partial x_i} [\lambda(\vec{r}) \nabla \cdot \bar{u}(\vec{r})], \quad (1)$$

where \bar{u} is the displacement field. In general, \bar{u} can be decoupled into a longitudinal part and a transverse part, i.e. $\bar{u} = \nabla \phi_l + \nabla \times (\phi_t \hat{e}_z)$, where ϕ_l and ϕ_t are the longitudinal and transverse gauge potentials, respectively.

2.1 Single-scattering, the scattering coefficients

If there is only one scatterer, the solutions to ϕ_l and ϕ_t can be expanded by using Bessel and Hankel functions. The wave incident on a single scatterer, p , is:

$$\bar{u}_p^{inc}(\vec{r}_p) = \sum_m \left(a_{lm}^p \nabla \left[J_m(k_{l0} r_p) e^{im\theta_p} \right] + a_{tm}^p \nabla \times \left[\hat{z} J_m(k_{t0} r_p) e^{im\theta_p} \right] \right), \quad (2)$$

and the wave scattered by the same scatterer is

$$\bar{u}_p^{sca}(\vec{r}_p) = \sum_m \left(b_{lm}^p \nabla \left[H_m^{(1)}(k_{l0} r_p) e^{im\theta_p} \right] + b_{tm}^p \nabla \times \left[\hat{z} H_m^{(1)}(k_{t0} r_p) e^{im\theta_p} \right] \right), \quad (3)$$

where $J_m(x)$ and $H_m^{(1)}(x)$ are Bessel functions and Hankel functions of the first kind, respectively.

$k_{l0} = \omega\sqrt{\rho_0/(\kappa_0 + \mu_0)}$ and $k_{t0} = \omega\sqrt{\rho_0/\mu_0}$ represent the longitudinal and transverse wave vectors in the matrix, respectively. ω is the angular frequency. $\vec{r}_p = (r_p, \theta_p)$ are the polar coordinates originating at the center of the scatterer. The longitudinal and transverse waves in the matrix are coupled by the scatterings of the scatterers, inside which the displacement is given by:

$$\bar{u}_p(\vec{r}_p) = \sum_m \left(c_{lm}^p \nabla \left[J_m(k_{ls}r_p) e^{im\theta_p} \right] + c_{tm}^p \nabla \times \left[\hat{z} J_m(k_{ts}r_p) e^{im\theta_p} \right] \right), \quad (4)$$

where $k_{ls} = \omega\sqrt{\rho_s/(\kappa_s + \mu_s)}$ and $k_{ts} = \omega\sqrt{\rho_s/\mu_s}$ are the longitudinal and transverse wave vectors inside the scatterer, respectively. The coefficients of those Bessel and Hankel functions can be determined by considering the elastic boundary conditions which are the continuities of the radial and tangential component of the displacement field, i.e., u_r and u_θ , and the continuities of the stresses, σ_{rr} and $\sigma_{r\theta}$, at the interface. These continuities on the surface of a cylinder relate b_{lm}^p and b_{tm}^p to a_{lm}^p and a_{tm}^p through:

$$b_{\alpha m}^p = \sum_{\beta=l,t} \sum_{m'} t_{\alpha\beta mm'} a_{\beta m'}^p \quad (\alpha = l, t), \quad (5)$$

where $t_{\alpha\beta mm'} = D_m^{\alpha\beta} \delta_{mm'}$. $D_m^{\alpha\beta}$ are elastic Mie-like scattering coefficients for isotropic scatterers and are functions of k_{ls} , k_{ts} , k_{l0} , k_{t0} and r_s . The explicit expressions for $D_m^{\alpha\beta}$ can be found in (Wu et al., 2007).

2.2 Periodic structures and multiple-scattering

For a collection of scatterers, the MST takes full account of the multiple scatterings between any two scatterers (Liu et al., 2000a; Mei et al., 2003). The wave incident on the scatterer p is contributed by two parts: one is the external incident waves from outside the system, and the other part is the scattered waves coming from all the other scatterers inside the system. Thus, the total incident waves on the scatterer p are expressed as:

$$\begin{aligned} \bar{u}_p^{inc}(\vec{r}_p) = & \sum_m \left(a_{lm}^{p0} \nabla \left[J_m(k_{l0}r_p) e^{im\theta_p} \right] + a_{tm}^{p0} \nabla \times \left[\hat{z} J_m(k_{t0}r_p) e^{im\theta_p} \right] \right) \\ & + \sum_{q \neq p} \sum_{m''} \left(b_{lm''}^q \nabla \left[H_{m''}^{(1)}(k_{l0}r_q) e^{im''\theta_q} \right] + b_{tm''}^q \nabla \times \left[\hat{z} H_{m''}^{(1)}(k_{t0}r_q) e^{im''\theta_q} \right] \right), \end{aligned} \quad (6)$$

where (r_q, θ_q) denote \vec{r}_q in the polar coordinates originating at the center of scatterer q . Here \vec{r}_q and \vec{r}_p refer to the same spatial point measured from the positions of scatterers q and p , respectively. For simplicity, the center of scatterer p is chosen as the origin and the position of scatterer q is denoted by $\vec{R}_{qp} = (R_{qp}, \Theta_{qp})$. Thus, $\vec{r}_q = \vec{r}_p - \vec{R}_{qp}$. The relation between \vec{r}_p , \vec{r}_q and \vec{R}_{qp} is depicted in Fig. 1.

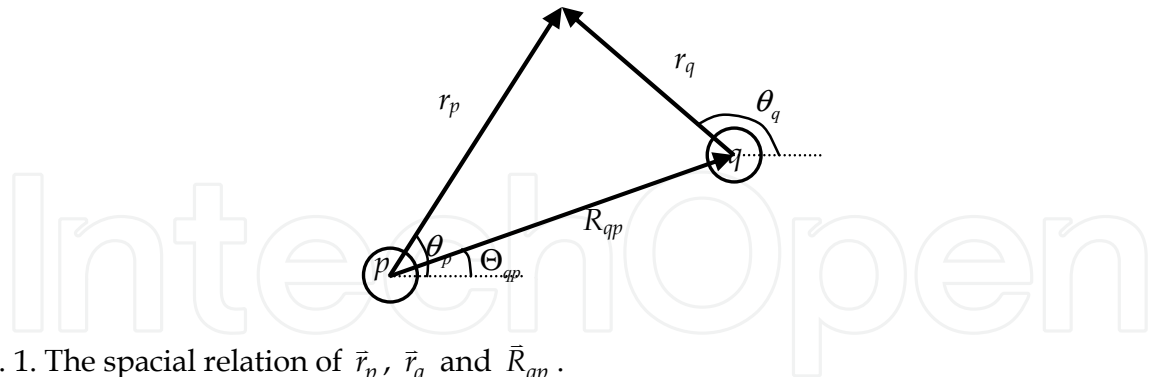


Fig. 1. The spacial relation of \vec{r}_p , \vec{r}_q and \vec{R}_{qp} .

With the help of Graf's addition theorem (Abramowitz & Stegun, 1972), the Hankel functions depicting the scattered wave coming from the scatterer q can be changed into Bessel functions describing the wave incident on the scatterer p , which is:

$$H_{m''}^{(1)}(k_{\alpha 0} r_q) e^{im''\theta_q} = \sum_m g_{mm''}^{\alpha} J_m(k_{\alpha 0} r_p) e^{im\theta_p} \quad (\alpha = l, t), \quad (7)$$

where

$$g_{mm''}^{\alpha} = H_{m-m''}^{(1)}(k_{\alpha 0} R_{qp}) e^{i(m''-m)\theta_{qp}} \quad (\alpha = l, t) \quad (8)$$

Substituting Eqs. (7) and (8) into (6), we obtain:

$$\begin{aligned} \vec{u}_p^{inc}(\vec{r}_p) = & \sum_m \left(a_{lm}^{p0} + \sum_{q \neq p} \sum_{m''} b_{lm''}^q g_{mm''}^l \right) \nabla \left[J_m(k_{l0} r_p) e^{im\theta_p} \right] \\ & + \sum_m \left(a_{tm}^{p0} + \sum_{q \neq p} \sum_{m''} b_{tm''}^q g_{mm''}^t \right) \nabla \times \left[\hat{z} J_m(k_{t0} r_p) e^{im\theta_p} \right] \end{aligned} \quad (9)$$

Eq. (2) together with Eqs. (5) and (9) leads to the following self-consistent equation:

$$b_{\alpha m}^p = \sum_{\beta=l,t} \sum_{m'} t_{\alpha\beta m m'} \left(a_{\beta m'}^{p0} + \sum_{q \neq p} \sum_{m''} g_{m'm''}^{\beta} b_{\beta m''}^q \right) \quad (10)$$

This set of self-consistent equations can be written into the standard form of linear equations $Ax = B$, and the multiple-scattering problem is numerically solved.

If the scatterers are arranged in a periodic array, the Bloch theorem, $b_{\alpha m''}^q = b_{\alpha m}^p e^{i\vec{K} \cdot \vec{R}_{qp}}$ ($\alpha = l, t$), can be applied, where \vec{K} is the Bloch wave vector. For an eigenvalue problem, the external incident field is dropped off so that Eq. (10) is converted into:

$$\sum_{\beta=l,t} \sum_m \left(\sum_{m'} t_{\alpha\beta mm'} \sum_{q \neq p} g_{m'm}^\beta e^{i\vec{K} \cdot \vec{R}_q} - \delta_{mm'} \right) b_{\beta m}^p = 0 \quad (11)$$

Eq. (11) has nontrivial solutions if and only if,

$$\det \left| \sum_{m'} t_{\alpha\beta mm'} S(\beta, m' - m) - \delta_{mm'} \right| = 0, \quad (12)$$

where

$$S(\beta, m' - m) = \sum_{q \neq p} g_{m'm}^\beta e^{i\vec{K} \cdot \vec{R}_q}$$

represents lattice sums. The solution of Eq. (12) offers the dependence of frequency, ω , on the Block wave vector, \vec{K} , which is known as the dispersion relation. To solve Eq. (12) for dispersion relations, one needs to evaluate the lattice sums first, which can be accomplished through several techniques (Chin et al., 1994; Mei et al., 2003). The expression of $S(\beta, m' - m)$ is given by (Wu and Z. Zhang, 2009):

$$S(\beta, n) = \frac{4i^{n+1} k_{\beta 0}}{\Omega J_{n+1}(k_{\beta 0} a)} \sum_h \frac{J_{n+1}(Q_h a)}{Q_h (k_{\beta 0}^2 - Q_h^2)} e^{in\varphi_h} - \left(H_1^{(1)}(k_{\beta 0} a) + \frac{2i}{\pi k_{\beta 0} a} \right) \delta_{n,0}, \quad (n \geq 0) \quad (13)$$

$$S(\beta, -n) = -S^*(\beta, n)$$

where a denotes the lattice constant, Ω is the volume of the unit cell and (Q_h, φ_h) stands for the vector $\vec{Q}_h = \vec{K} + \vec{K}_h$ in polar coordinates, and \vec{K}_h is the reciprocal lattice vector.

3. Symmetry properties of elastic metamaterials

Since the MST is capable of producing accurate dispersion relations for all frequencies, it is a good approach in the study of the symmetry properties of an elastic metamaterial. The elastic metamaterial is isotropic if its dispersion relation, $\omega(\vec{K})$, does not depend on the direction of \vec{K} . In the framework of MST, the dispersion relation can be calculated numerically by solving Eq. (12). In the long wavelength limit, both Ka and $k_0 a$ are all much smaller than unity and appropriate approximations can be made in the Bessel and Hankel functions in the lattice sum $S(\beta, m' - m)$ and the scattering matrix $t_{\alpha\beta mm'}$. This simplifies the secular equation and benefits the derivation of analytic expression of EMT.

Taking $J_n(x) \cong x^n / (2^n n!)$, $H_0^{(1)}(x) \cong 2 \ln x / \pi$ and $H_n^{(1)}(x) \cong -2^n (n-1)! / (\pi x^n)$ for $x = k_{l0} r_s$, $k_{t0} r_s$, $k_{l0} a$, $k_{t0} a$ and Ka in Eq. (12), it is easy to find that the leading terms are those with $|m| \leq 2$, where m corresponds to the order of Bessel and Hankel functions and is called the angular quantum number. Thus, we only need to consider the terms with $0 \leq n \leq 4$ in Eq. (13), in which the summation

$$\sum_h J_{n+1}(Q_h a) e^{in\varphi_h} / [Q_h (k_{\beta 0}^2 - Q_h^2)]$$

can be separated into two terms: the first is $\bar{K}_h = 0$ or $\bar{Q}_h \cong \bar{K}$, the second is the sum of all other terms with $\bar{K}_h \neq 0$ or $\bar{Q}_h \cong \bar{K}_h$. Then, the lattice sum takes the following expression:

$$S(\beta, n) \cong \frac{4i^{n+1}}{\Omega} \left(\frac{K^n}{k_{\beta 0}^n (k_{\beta 0}^2 - K^2)} e^{-in\phi_k} + \frac{k_{\beta 0} 2^{n+1} (n+1)!}{(k_{\beta 0} a)^{n+1}} \sum_{h(K_h \neq 0)} \frac{J_{n+1}(K_h a)}{K_h (k_{\beta 0}^2 - K_h^2)} e^{-in\phi_{kh}} \right), \quad (0 \leq n \leq 4) \quad (14)$$

$$S(\beta, -n) = -S^*(\beta, n),$$

where (K_h, ϕ_{kh}) denotes the polar coordinates of \bar{K}_h , the reciprocal lattice vector of the lattice. The summation of all nonzero reciprocal lattice vectors in the second term in the bracket reveals the dependence of lattice sum on the lattice structure, which influences the symmetry properties of the dispersion relations.

3.1 Isotropic dispersions

For a 2D hexagonal lattice with a lattice constant a , the reciprocal lattice follows:

$$\bar{K}_h = \frac{4\pi}{\sqrt{3}a} \left(h_i \hat{i} + h_j \left(\frac{1}{2} \hat{i} + \frac{\sqrt{3}}{2} \hat{j} \right) \right); \quad h_i, h_j \in Z \quad (15)$$

Here, \hat{i} and \hat{j} represent the unit vectors along the x - and y -axes in the reciprocal space. When $n \neq 0$, due to the symmetry of a hexagonal lattice, the summation in the second term of Eq. (14) is zero, which can be proved in the following way. For an arbitrarily chosen reciprocal lattice vector, (K_{h1}, ϕ_{kh1}) , there always exist five other reciprocal lattice vectors at $(K_{h1}, \phi_{kh1} + N\pi/3)$, $N = 1, 2, 3, 4, 5$ such that $\sum_{N=0}^5 e^{-inN\pi/3} = 0$. Thus, the summation in Eq. (14) vanishes after summing over all the non-zero \bar{K}_h and only the first term of Eq. (14) survives. When $n = 0$, the second term in Eq. (14) no longer sums to zero as $e^{-in\phi_{kh}} = 1$. However, this term can be ignored in the long wavelength limit because compared to the first term in Eq. (14) which is on the order of ω^{-2} , it is on the order of ω^0 . Thus, Eq. (14) is further reduced to:

$$S(\beta, n) \cong \frac{8i^{n+1} K^n}{\sqrt{3} a^2 k_{\beta 0}^n (k_{\beta 0}^2 - K^2)} e^{-in\phi_k}, \quad 0 \leq n \leq 4 \quad (16)$$

Substituting Eq. (16) into Eq.(12), we find the following two roots:

$$(K_1^{\text{tri}})^2 = F_1(\tilde{D}_1^{\text{II}})F_2(\tilde{D}_2^{\text{II}}) \quad \text{and} \quad (K_2^{\text{tri}})^2 = F_1(\tilde{D}_1^{\text{II}})F_3(\tilde{D}_2^{\text{II}}, \tilde{D}_0^{\text{II}}), \quad (17)$$

with

$$F_1(\tilde{D}_1^{\text{II}}) = -\frac{16i\tilde{D}_1^{\text{II}}(\kappa_0 + \mu_0) - \sqrt{3}a^2\omega^2\rho_0}{\sqrt{3}a^2},$$

$$F_2(\tilde{D}_2^{\parallel}) = -\frac{4\tilde{D}_2^{\parallel}(\kappa_0 + \mu_0)(\kappa_0 + 2\mu_0) + i\frac{\sqrt{3}}{2}a^2\omega^2\mu_0\rho_0}{\mu_0\left(4\tilde{D}_2^{\parallel}\kappa_0(\kappa_0 + \mu_0) - i\frac{\sqrt{3}}{2}a^2\omega^2\mu_0\rho_0\right)}, \quad (18)$$

$$F_3(\tilde{D}_2^{\parallel}, \tilde{D}_0^{\parallel}) = -\frac{\left(4\tilde{D}_0^{\parallel}(\kappa_0 + \mu_0) + i\frac{\sqrt{3}}{2}a^2\omega^2\rho_0\right)\left(4\tilde{D}_2^{\parallel}(\kappa_0 + \mu_0)(\kappa_0 + 2\mu_0) + i\frac{\sqrt{3}}{2}a^2\omega^2\mu_0\rho_0\right)}{(\kappa_0 + \mu_0)\left(32\tilde{D}_0^{\parallel}\tilde{D}_2^{\parallel}\mu_0(\kappa_0 + \mu_0)^2 - i\frac{\sqrt{3}}{2}a^2\omega^2\rho_0\left(4\tilde{D}_2^{\parallel}\kappa_0(\kappa_0 + \mu_0) - i\frac{\sqrt{3}}{2}a^2\omega^2\mu_0\rho_0\right)\right)},$$

where \tilde{D}_m^{\parallel} is the Mie-like scattering coefficient D_m^{\parallel} after taking the long wavelength approximation. It is obviously seen that the roots $(K_1^{\text{tri}})^2$ and $(K_2^{\text{tri}})^2$ given in Eq. (17) do not depend on the direction of \vec{K} , i.e., ϕ_K . This implies that all the dispersion relation for an elastic metamaterial with a hexagonal structure are isotropic near the Γ point in the long wavelength limit.

3.2 Anisotropic dispersions

For the case of a square lattice, the lattice sum is almost the same as that of the hexagonal lattice case except for the $n \neq 0$ case. The reciprocal lattice vector of a square lattice is expressed by:

$$\vec{K}_h = \frac{2\pi}{a}(h_i\hat{i} + h_j\hat{j}); h_i, h_j \in \mathcal{Z} \quad (19)$$

For an arbitrarily chosen reciprocal lattice vector (K_{h1}, ϕ_{Kh1}) , there always exist the other three at

$$(K_{h1}, \phi_{Kh1} + N\pi/2), N = 1, 2, 3, \text{ which makes the summation } \sum_{N=0}^3 e^{-inN\pi/2}$$

cancel to zero when $1 \leq n \leq 3$, and equals to 4 when $n = 4$ respectively. This indicates that the second term of Eq. (14) only vanishes when $1 \leq n \leq 3$. Thus, in the long wavelength limit, the lattice sum can be written, as

$$S(\beta, n) \cong \frac{4i^{n+1}K^n}{a^2k_{\beta 0}^n(k_{\beta 0}^2 - K^2)} e^{-in\phi_K} \quad (0 \leq n \leq 3) \quad (20)$$

for $0 \leq n \leq 3$, and

$$S(\beta, 4) \cong \left(\frac{4iK^4}{a^2k_{\beta 0}^4(k_{\beta 0}^2 - K^2)} + \gamma_{\beta} e^{i4\phi_K} \right) e^{-i4\phi_K} \quad (21)$$

for $n = 4$, where

$$\gamma_\beta = \frac{16 \cdot 2^5 \cdot 5! i}{a^6 k_{\beta 0}^4} \left(\sum_{h_j=0}^N \sum_{h_i=1}^N \frac{J_5 \left(2\pi \sqrt{h_i^2 + h_j^2} \right) e^{i4 \arctan(h_j/h_i)}}{2\pi \sqrt{h_i^2 + h_j^2} \left(k_{\beta 0}^2 - \left(\frac{2\pi}{a} \right)^2 (h_i^2 + h_j^2) \right)} \right) \quad (22)$$

Due to the non-zero γ_β term in Eq. (22), the determinant in Eq. (12) is ϕ_K -dependent, which gives rise to anisotropic dispersion relations. The explicit expressions for K_1^{squ} and K_2^{squ} are very complicated and will be further discussed in the next Section.

4. Effective medium theory for elastic metamaterials

The MST method is capable of producing the dispersion relations of an elastic metamaterial so that the effective wave speed for elastic waves in the metamaterial can be obtained accordingly. However, it is not able to provide an effective description for each parameters. Knowing the effective parameters will provide a clear theoretical explanation of the unusual phenomenon of a metamaterial and greatly benefit the design of new metamaterials. This Section is devoted to the derivation of EMTs.

4.1 Isotropic media: Coherent potential approximation approach

If the elastic metamaterial is isotropic, i.e., cylinders arranged in a hexagonal lattice, the EMT can be derived by considering the scattering of elastic waves by a coated cylinder embedded in the effective medium with effective parameters $(\kappa_e, \mu_e, \rho_e)$, which is shown in Figure 2 (Wu et al., 2007). The coated cylinder consists of the scatterer surrounded by a layer of the matrix. The inner and outer radii, which are denoted by r_s and r_0 , respectively, satisfy $r_s^2 / r_0^2 = p$, where p is the filling ratio of the scatterer. The effective parameters κ_e , μ_e and ρ_e are determined by the condition that the total scattering of the coated cylinder vanishes which is so-called CPA. This condition together with the boundary conditions on the surface of the coated cylinder at $r = r_0$, provides another two relations: $b_{lm} = D_m^{ll}(e)a_{lm} + D_m^{lt}(e)a_{tm}$ and $b_{tm} = D_m^{tl}(e)a_{lm} + D_m^{tt}(e)a_{tm}$, where $D_m^{\alpha\beta}(e)$ ($\alpha, \beta = l, t$) can be obtained by replacing λ_s , ρ_s , μ_s , k_{ls} , k_{ts} and r_s in $D_m^{\alpha\beta}$ ($\alpha, \beta = l, t$) mentioned in Section 2.1 with λ_e , ρ_e , μ_e , k_{le} , k_{te} and r_0 , respectively, where k_{le} (k_{te}) are the longitudinal (transverse) wave vectors in the effective medium. These relations together with the relations between $b_{\alpha m}$ and $a_{\alpha m}$ ($\alpha = l, t$) shown in Section 2.1 give the following effective medium condition:

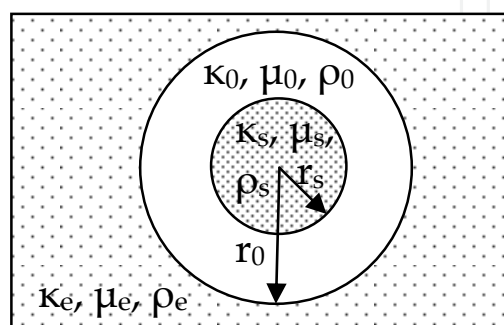


Fig. 2. Micro-structure of the effective medium. (Wu et al., 2007)

$$D_m^{\alpha\beta}(e) = D_m^{\alpha\beta} \quad (\alpha, \beta = l, t) \quad (23)$$

In the long wavelength limit, where $k_{l0}r_0 \ll 1$, $k_{t0}r_0 \ll 1$, $k_{le}r_0 \ll 1$ and $k_{te}r_0 \ll 1$, Eq. (23) can be simplified into the following effective medium equations for the elastic metamaterial:

$$\frac{(\kappa_0 - \kappa_e)}{(\mu_0 + \kappa_e)} = \frac{4\tilde{D}_0^{ll}}{i\pi r_0^2 k_{l0}^2}, \quad (24)$$

$$\frac{(\rho_0 - \rho_e)}{\rho_0} = -\frac{8\tilde{D}_1^{ll}}{i\pi r_0^2 k_{l0}^2}, \quad (25)$$

$$\frac{\mu_0(\mu_0 - \mu_e)}{(\kappa_0\mu_0 + (\kappa_0 + 2\mu_0)\mu_e)} = \frac{4\tilde{D}_2^{ll}}{i\pi r_0^2 k_{l0}^2} \quad (26)$$

Obviously, κ_e , ρ_e and μ_e are independently determined by \tilde{D}_m^{ll} of the embedded cylinders alone with angular quantum numbers $m = 0, 1$ and 2 .

The dispersion relation can be reproduced from effective medium parameters. Comparing Eqs. (24)-(26) to Eqs. (17) and (18), it is easy to show that ρ_e/μ_e coincides with $(K_1^{tri}/\omega)^2$ and $\rho_e/(\kappa_e + \mu_e)$ is identical to $(K_2^{tri}/\omega)^2$. The equivalence provides a strong evidence that the dispersion relation is isotropic for a hexagonal lattice and its effective medium properties can be evaluated from the EMT derived from CPA.

Eqs. (24)-(26) require the wavelengths in both the host and the effective medium to be much larger than the size of the unit cell, but they do not impose any restriction on the wavelengths inside the scatterer. If the condition of $k_{ls}r_s \ll 1$, $k_{ts}r_s \ll 1$ is further considered, the quasi-static limit is reached and Eqs. (24)-(26) becomes:

$$\frac{(\kappa_0 - \kappa_e)}{(\mu_0 + \kappa_e)} = p \frac{(\kappa_0 - \kappa_s)}{(\mu_0 + \kappa_s)}, \quad (27)$$

$$(\rho_0 - \rho_e) = p(\rho_0 - \rho_s), \quad (28)$$

$$\frac{(\mu_0 - \mu_e)}{(\kappa_0\mu_0 + (\kappa_0 + 2\mu_0)\mu_e)} = p \frac{(\mu_0 - \mu_s)}{(\kappa_0\mu_0 + (\kappa_0 + 2\mu_0)\mu_s)} \quad (29)$$

The 3D version was reported by Berryman decades ago (Berryman, 1980). It should be pointed out that elastic EMT cannot recover the acoustic EMT by setting all the shear moduli to be zero, because of the different boundary conditions of elastic and acoustic waves.

Figure 3 shows the equifrequency surface (EFS) of a hexagonal array of silicone rubber cylinders with radii of $0.2a$ embedded in an epoxy host. An EFS is a collection of all states in the \vec{K} space that have the same frequency. The metamaterial is isotropic if its EFS is a circle. Here the dimensionless frequency, $\tilde{f} = (\omega a)/(2\pi c_{t0})$, is used, where c_{t0} is the

transverse wave speed inside the host. The silicone rubber's material parameters are $\rho = 1.3 \times 10^3 \text{ kg/m}^3$, $\lambda = 6 \times 10^5 \text{ N/m}^2$ and $\mu = 4 \times 10^4 \text{ N/m}^2$, which means the wave speeds inside the rubber are: 22.87 m/s for longitudinal waves and 5.54 m/s for transverse waves. The corresponding parameters in the epoxy host are $\rho = 1.18 \times 10^3 \text{ kg/m}^3$, $\lambda = 4.43 \times 10^9 \text{ N/m}^2$ and $\mu = 1.59 \times 10^9 \text{ N/m}^2$, which indicates the wave speeds are 2539.52 m/s (1160.80 m/s) for longitudinal (transverse) waves (Liu et al., 2000b). Apparently, slow wave speeds imply that wavelengths inside the silicone rubber cylinder may be comparable to or even much smaller than the size of the cylinder at low frequencies. Thus, Mie-like resonances may occur, which serve as the built-in resonances required for metamaterials. Here the frequency \tilde{f} is chosen to be 0.03 where both $k_{ls}r_s \approx 1.9$ and $k_{ts}r_s \approx 7.9$ are larger than unity indicating it is not in the quasi-static limit. Figure 3(a) shows the corresponding EFS, which exhibits two circular rings, with the inner one denoting the quasi-longitudinal branch and the outer one representing the quasi-transverse branch. The corresponding Ka as a function of ϕ_k is plotted in Fig. 3(b) by open circles. These circles form two horizontal lines, indicating dispersions are isotropic, i.e., effective wave speeds do not vary with directions. Also plotted in Fig. 3(b) are the results of EMT calculated from Eq. (17) or Eqs. (24)-(26), depicted by two solid lines. The complete overlaps between solid lines and circles give a numerical support to the correctness of the EMT in the long wavelength limit.

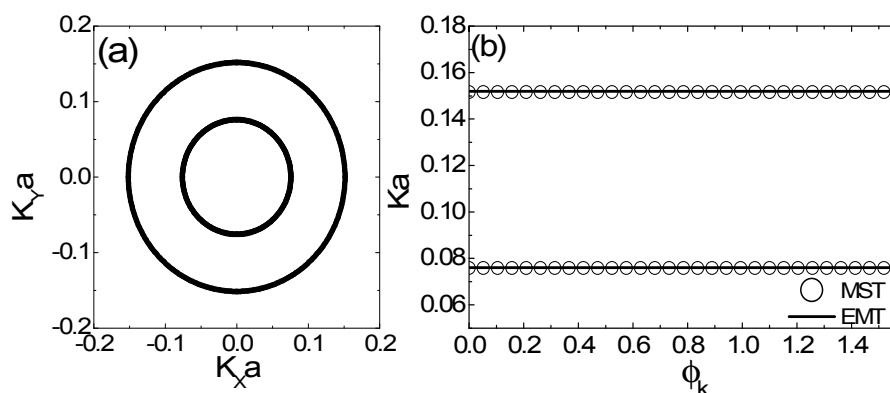


Fig. 3. (a) The equifrequency surface for a hexagonal array. (b) Ka as a function of ϕ_k . (Wu & Z. Zhang, 2009)

4.2 Anisotropic media: Christoffel's equation

If the elastic metamaterial is anisotropic, such as cylindrical scatterers arranged in a square lattice, the CPA fails as it only deals with isotropic cases. In this case, the result of MST, i.e., Eq. (14), can give an anisotropic EMT in the form of Christoffel's equation.

Taking the long wavelength limit approximation on Eq. (12) and plug in Eqs. (20) and (22), the expressions for K_1^{squ} and K_2^{squ} can be written as the solutions of the following Christoffel's equation for an anisotropic medium (Royer & Dieulesaint, 1999)

$$\det \begin{vmatrix} \cos^2 \phi_K C_{11} \rho_e^{-1} + \sin^2 \phi_K C_{44} \rho_e^{-1} - (\omega/K)^2 & \cos \phi_K \sin \phi_K (C_{12} + C_{44}) \rho_e^{-1} \\ \cos \phi_K \sin \phi_K (C_{12} + C_{44}) \rho_e^{-1} & \cos^2 \phi_K C_{44} \rho_e^{-1} + \sin^2 \phi_K C_{11} \rho_e^{-1} - (\omega/K)^2 \end{vmatrix} = 0 \quad (30)$$

where ϕ_K denotes the angle between the Bloch wave vector \vec{K} and the x -axis, and ρ_e is the effective mass density derived from CPA. It is convenient to express the three effective moduli in Eq. (32) in terms of the two effective parameters κ_e and μ_e shown in Eqs. (26) and (28) for isotropic media,

$$C_{11} = \kappa_e + \mu_e + \Delta_1, \quad (31)$$

$$C_{12} = \kappa_e - \mu_e - \Delta_1, \quad (32)$$

$$C_{44} = \mu_e + \Delta_2, \quad (33)$$

where $\Delta_{1,2} = \delta(\mu_0 - \mu_e)^2 / [\delta(\mu_0 - \mu_e) \mp 8\rho_0]$, with $-$ and $+$ for Δ_1 and Δ_2 , respectively. Here $\delta = i(k_{t0}^4 \gamma_l - k_{t0}^4 \gamma_t) a^2 / \omega^2$ and $\gamma_{l,t}$ is given by Eq.(22). It is clear that Δ_1 and Δ_2 are responsible for the anisotropy. In the long wavelength limit, δ has the following expression:

$$\delta = -\frac{1920}{\pi^5} \frac{\kappa_0 \rho_0}{\mu_0 (\kappa_0 + \mu_0)} \left(\sum_{h_j=0}^N \sum_{h_i=1}^N \frac{J_5 \left(2\pi \sqrt{h_i^2 + h_j^2} \right) e^{i4 \arctan(h_j/h_i)}}{\left(\sqrt{h_i^2 + h_j^2} \right)^5} \right) \quad (34)$$

Eq. (30) gives:

$$\left(\frac{\omega}{K_1} \right)^2 = \frac{1}{2\rho_e} \left(C_{11} + C_{44} - \sqrt{\sin^2(2\phi_K)(C_{12} + C_{44})^2 + \cos^2(2\phi_K)(C_{11} - C_{44})^2} \right), \quad (35)$$

$$\left(\frac{\omega}{K_2} \right)^2 = \frac{1}{2\rho_e} \left(C_{11} + C_{44} + \sqrt{\sin^2(2\phi_K)(C_{12} + C_{44})^2 + \cos^2(2\phi_K)(C_{11} - C_{44})^2} \right) \quad (36)$$

Since the origin of anisotropy comes from the term $\gamma_\beta \neq 0$, the isotropy is expected to recover when $\gamma_\beta = 0$ (or $\delta = 0$). In this case, $C_{11} = C_{12} + 2C_{44}$ (Royer & Dieulesaint, 1999) and Eqs. (35) and (36) can be reduced to $(\omega/K_1)^2 = \mu_e/\rho_e$ and $(\omega/K_2)^2 = (\kappa_e + \mu_e)/\rho_e$, which are the square of two known wave speeds. For the case of anisotropic dispersions, Eqs. (35) and (36) give the dispersion relations for the quasi-transverse and quasi-longitudinal bands (Royer & Dieulesaint, 1999). Eq. (35) shows that $(\omega/K_1)^2$ oscillates between two extrema, $(\mu_e + \Delta_2)/\rho_e$ and $(\mu_e + \Delta_1)/\rho_e$ at $\phi_K = 0$ and $\pi/4$, respectively. Similarly, $(\omega/K_2)^2$ oscillates between its two extrema, $(\kappa_e + \mu_e + \Delta_1)/\rho_e$ and $(\kappa_e + \mu_e + \Delta_2)/\rho_e$. If both $|\Delta_1|$ and $|\Delta_2|$ are much smaller than $|\mu_e|$ and $|\kappa_e + \mu_e|$, and the amplitude of the oscillation, $|\Delta_1 - \Delta_2|$, is small, the angle averaged dispersions, $(\omega/K_1)^2$ and $(\omega/K_2)^2$, can be well approximated by μ_e/ρ_e and $(\kappa_e + \mu_e)/\rho_e$, which are the results of isotropic EMT given by Eqs. (24)-(26).

Figure 4(a) is the same as Figure 3(a), but the rubber cylinders are arranged in a square array. The inner ring represents the quasi-longitudinal branch with distinct anisotropy and the outer one is the quasi-transverse branch with weak anisotropy. The corresponding Ka

as a function of ϕ_K is plotted in Fig. 4(b) in open circles, which form two oscillating curves induced by the γ_β term in Eq. (21). In this case, $\Delta_1 = 0.0158$ and $\Delta_2 = -0.0179$ (in the unit of μ_0), which are very small compared to κ_e (2.241) and μ_e (0.733). $(\omega / K_1)^2$ and $(\omega / K_2)^2$ should reach their maximum and minimum at $\phi_K = 0$, respectively. This implies K_1 (K_2) is at its minimum (maximum). Also, K_1 arrives at its maximum at $\phi_K = \pi / 4$, where K_2 takes its minimal value. These are clearly illustrated Fig. 4(b). If we use the ratio $d_i = (K_i^{\max} - K_i^{\min}) / \langle K_i \rangle, (i = 1, 2)$ to characterize the amount of anisotropy (Ni and Cheng, 2005), where K_i^{\max}, K_i^{\min} and $\langle K_i \rangle$ are the maximum, minimum and average of K_i , the corresponding quantities are $d_1 = 5.39\%$ and $\langle K_1 a \rangle = 0.1603$ for the transverse waves and $d_2 = 1.20\%$ and $\langle K_2 a \rangle = 0.0793$ for the longitudinal waves. The averaged values of $K_i a$ coincide with the results calculated from the isotropic effective medium, i.e., Eq. (24)-(26), which give $K_t a = 0.1599$ and $K_l a = 0.0794$ as shown in Fig. 4 (b) in two horizontal solid lines. Fig. 4(b) demonstrates that the isotropic EMT can well predict the angle-averaged value of $K_i a$ in the case of anisotropy.

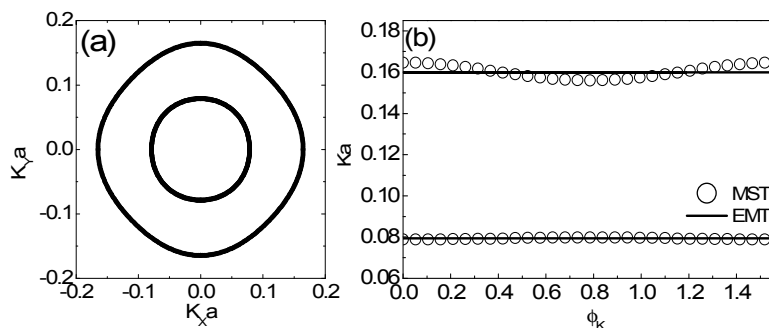


Fig. 4. The same as Figure 3 but the lattice is a square lattice. (Wu & Z. Zhang, 2009)

5. Design of elastic metamaterials

The purpose of deriving EMTs is to reveal the relationship between the resonances of the microstructures and the effective parameters and to provide a guide in the design of new metamaterials with novel properties. Even for isotropic metamaterials, the negativities in three effective parameters as well as their combinations can give rise to various interesting properties unseen in natural materials. For instance, since the effective phase velocities in 2D elastic metamaterials are $c_{le} = \sqrt{\kappa_e + \mu_e} \sqrt{1/\rho_e}$ and $c_{te} = \sqrt{\mu_e} \sqrt{1/\rho_e}$ for longitudinal and transverse waves, respectively, a single negative ρ_e in a frequency regime leads to imaginary c_{le} and c_{te} , which implies the existence of a band gap for both longitudinal and

	$\kappa_e + \mu_e > 0$ $\mu_e > 0$	$\kappa_e + \mu_e > 0$ $\mu_e < 0$	$\kappa_e + \mu_e < 0$ $\mu_e > 0$	$\kappa_e + \mu_e < 0$ $\mu_e < 0$
$\rho_e > 0$	$n_l > 0; n_t > 0$	$n_l > 0; t: \text{gap}$	$n_t > 0; l: \text{gap}$	$l \& t: \text{gap}$
$\rho_e < 0$	$l \& t: \text{gap}$	$n_t < 0; l: \text{gap}$	$n_l < 0; t: \text{gap}$	$n_l < 0; n_t < 0$

Table 1. Various wave propagation properties. Positive (negative) n indicates positive (negative) propagating bands. l and t represent longitudinal and transverse waves, respectively.

transverse waves (Liu et al., 2000b). On the other hand, a simultaneous negative ρ_e and μ_e (or $\kappa_e + \mu_e$) induces negative refractive index for the transverse (longitudinal) waves. Table 1 lists eight possible types of wave propagation in 2D elastic metamaterials with different combinations of signs in $\kappa_e + \mu_e$, ρ_e and μ_e . Like acoustic metamaterials (Li & Chan, 2004), the effective bulk modulus and shear modulus κ_e and μ_e determined according to Eqs. (24)-(26) do not satisfy the well-known bounds (Hashin & Shtrikman, 1963; Torquato, 1991) on the effective elastic moduli as these bounds are derived in the quasi-static limit. For anisotropic metamaterials, there exists at least one more effective elastic modulus which can also turn negative. Thus, many more interesting novel wave transport behaviors would be expected. Examples will be shown in a later section.

5.1 Isotropic elastic metamaterials

The simplest isotropic elastic metamaterial which is comprised of silicone rubber cylinders embedded in an epoxy host was exhibited in the last section. If the rubber cylinders' radii are chosen to be $0.3a$, it has been shown that various types of resonances were produced (Wu et al., 2007). The displacement fields for three typical resonances are plotted in Fig. 5, which clearly shows in (a), (b) and (c) the dipolar, quadrupolar and monopolar resonances. These resonances are linked to the effective medium parameters in the following manner implied by the EMT. The negative ρ_e arises from a dipolar resonance (\tilde{D}_1^{\parallel}), whereas the quadrupolar (\tilde{D}_2^{\parallel}) and monopolar (\tilde{D}_0^{\parallel}) resonances give rise to negative μ_e and negative κ_e , respectively. We can enlarge the negative regions of effective medium parameters by enhancing these resonances. For instance, the dipolar resonance shown in Fig. 5(a) exhibits the collective motion of the core part of rubber. This mode can be regarded as a simple "mass-spring" harmonic oscillator, with the central part serving as a "mass" and the boundary layer of the rubber serving as "spring". Replacing the inner region of rubber with another heavier cylinder, e.g. lead, will enhance the field oscillation of the silicone rubber, which, in turn, will widen the resonant region of ρ_e . This design was first proposed by Liu *et al* and was named as "locally resonant sonic materials" (Liu et al., 2000b), which were comprised of a cubic array of rubber-coated lead spheres embedded in epoxy. A large low-frequency band gap for both longitudinal and transverse waves, induced by negative mass

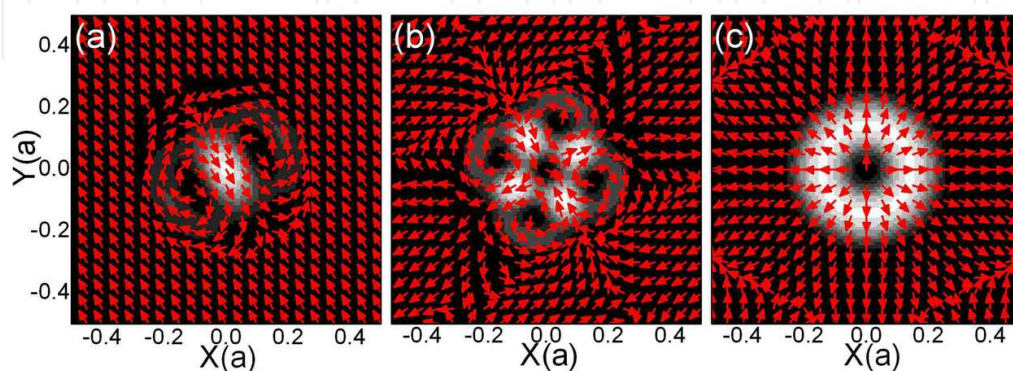


Fig. 5. Displacement fields for different resonances. The arrows represent the direction and the brightness denotes the amplitude, with white indicates larger. (Wu et al., 2007)

density, was found. Figure 5(c) exhibits the field pattern of a monopolar resonance, where the shape of the silicone rubber cylinder remains as a circle, with its cross-sectional area oscillating in time. This suggests that by making the inner core more easily compressed, we would enhance the monopolar resonance. This notion was supported by using air bubbles in water to achieve a large frequency region of negative bulk modulus (Ding et al., 2007). Figure 5(b) shows the relative motion of the rubber. This suggests that by making the core areas easier to deform, we would enhance the quadrupolar resonance so as to enlarge the negative region for shear modulus. An intuitive design is to make the rubber cylinder hollow. A metamaterial based on this design is made of rubber-coated air cylinders embedded in epoxy. The material parameters of air are given by $\rho = 1.23 \text{ kg/m}^3$ and $\lambda = 1.42 \times 10^{10} \text{ N/m}^2$. The effective medium parameters are evaluated by a generalized EMT, which uses the standard transfer-matrix method to obtain the quantities \tilde{D}_m^{ll} if the scatterers are layered cylinders.

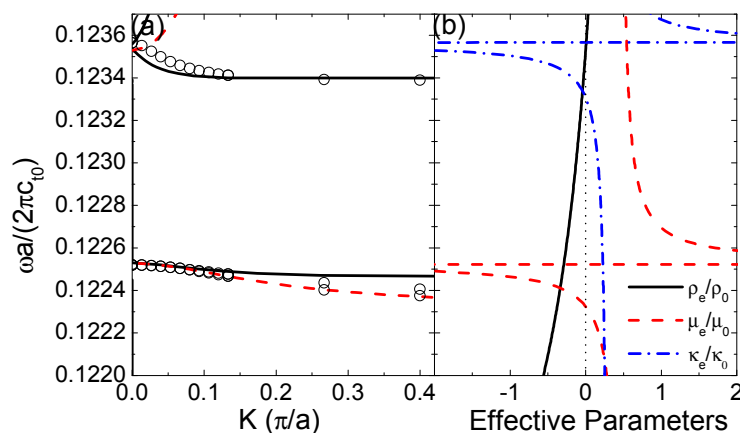


Fig. 6. Band structure and effective medium parameters for an array of hollow rubber cylinders embedded in epoxy. (Wu et al., 2007)

Figure 6(a) shows the band structure of hollow rubber cylinders embedded in epoxy in a hexagonal lattice. The inner and outer radii of hollow rubber cylinders are given as $r_{air} = 0.87r_s$ and $r_s = 0.3a$, which are carefully chosen so that a negative band for shear wave can be realized. The accurate MST results are plotted in open circles and the EMT predictions are featured by curves, with solid representing the longitudinal branch and dashed corresponding to the transverse branch. In the region of $0.12240 < \tilde{f} < 0.12253$, negative- n bands of both longitudinal and transverse waves are found, which implies that ρ_e , $\kappa_e + \mu_e$ and μ_e are all negative. These negative values are induced only by the resonances of ρ_e and μ_e as shown in Fig. 6(b), in which the individual effective medium parameters are plotted. In another region of $0.12340 < \tilde{f} < 0.12356$, negative- n band purely for longitudinal waves is found, which implies that ρ_e and $\kappa_e + \mu_e$ are both negative. These negative values arise from resonances of both ρ_e and κ_e . Figure 6(a) demonstrates that the isotropic EMT is still a good approximation even for complex scatterers with layered structures. The small discrepancies between the band-structure calculation and the effective medium prediction for the longitudinal branches shown in Fig. 6(a) is due to the less accurate approximation of the Hankel functions when the values of $k_{l0}r_0$ and $k_{t0}r_0$ are not much less than 1.

The structure of the hollow silicone rubber cylinder in epoxy does provide a frequency region of negative band for shear waves, but the bandwidth is too small to be of any practical use. Enlarging the quadrupolar resonance is a challenge task that has yet to be accomplished. Since replacing the inner part of the rubber by an easier deformed material is the direction, another common material, water, becomes a candidate. The material parameters of water are: $\rho = 1.0 \times 10^3 \text{ kg/m}^3$ and $\lambda = 2.22 \times 10^9 \text{ N/m}^2$. Figure 7 shows the effective medium parameters for the metamaterial with air core being replaced by water, which exhibits an improvement in the absolute bandwidth for negative shear modulus. However, the bandwidth to mid-frequency ratio (0.00145) is comparable to the previous air core case (0.00183). Moreover, the negative shear band disappears as the region for negative mass density does not overlap with that for negative shear modulus. This example demonstrates that simple replacement of air by water does not improve the negative shear band. Nevertheless, the replacement does enhance the dipolar resonance greatly in the very low frequency regime (which is not plotted here). This fact suggests that water core is a better candidate than air in the context of realizing negative mass density. The difficulty lies in increasing the negative region for shear modulus and adjusting it to overlap with that for the negative mass. This requires optimizing the inner and outer radii of the rubber cylinder. However, it can be shown that only altering the geometry parameters will not make a significant change.

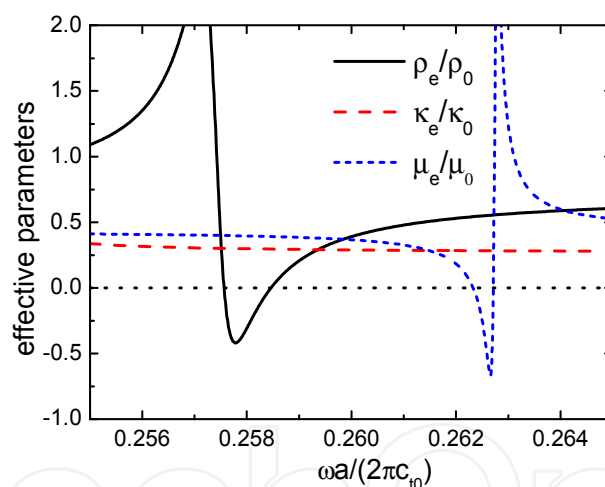


Fig. 7. Effective medium parameters for rubber-coated water cylinders embedded in epoxy in a hexagonal lattice.

Both Figs. 6(b) and 7 show that the μ resonance is very sharp, indicating that the energy is confined in the cylinders locally. To broaden the resonance, one strategy that could be adopted is to make the energy “spread” out of the cylinders so that resonances in different cylinders become “coupled” to each other. This can be realized by reducing the impedance mismatch between the rubber and the host.

Figure 8 shows the effective medium parameters for a rubber-coated water cylinder embedded in a foam host in a hexagonal lattice. The foam is polyethylene foam (HD115) whose material parameters are $\rho = 115 \text{ kg/m}^3$, $\lambda = 6.0 \times 10^6 \text{ N/m}^2$ and $\mu = 3.0 \times 10^6 \text{ N/m}^2$ (Zhou & Hu, 2009). The light foam makes the host more matched to the rubber than epoxy

which will benefit the enhancement of the resonance for shear modulus. It also makes the water-coated rubber core relatively heavier so that the resonance for mass density is also enhanced. By adjusting the geometric parameters to be $0.24a$ and $0.32a$ for inner and outer radii, respectively, a large frequency region, marked by "A" and "B" in Fig. 8, for both negative shear modulus and negative mass density is obtained. The bandwidth to mid-frequency ratio reaches 0.258, which is two orders of magnitude greater than the rubber-coated air cylinders in epoxy. The corresponding band structures as well as the transmission coefficients of a slab numerically calculated by MST are plotted in Fig. 9(a), which clearly shows a large negative band for transverse waves denoted by red dots and a narrow negative band for longitudinal waves denoted by blue dots. The polarization of these negative bands is determined through the transmission as shown in Fig. 9(b).

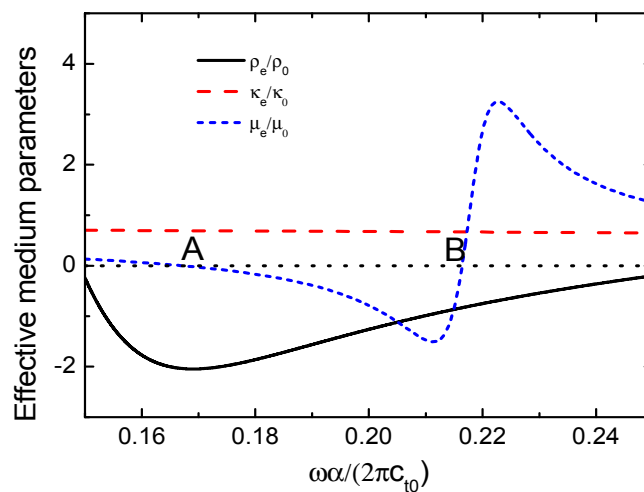


Fig. 8. Effective medium parameters for rubber-coated water cylinders embedded in foam in a hexagonal lattice.

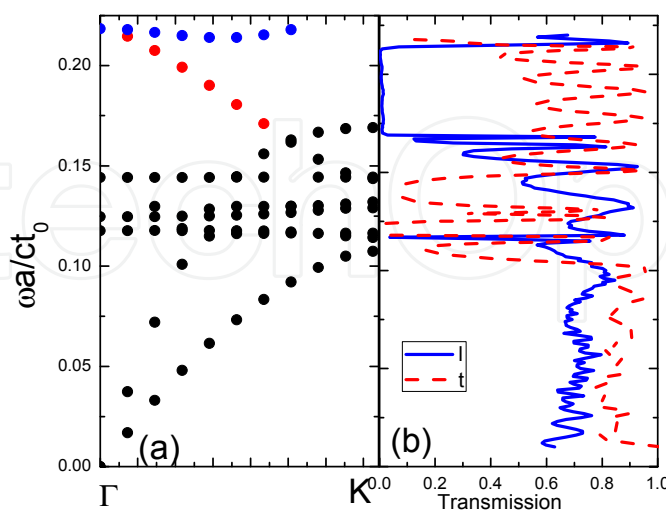


Fig. 9. (a) The dispersion along ΓK direction for the same system as Fig. 8.

(b) Transmission coefficients for longitudinal (solid blue) wave incident and transverse (dashed red) wave incident on a slab of width $6a$ and length $50a$. The incident wave is along ΓK direction. (Wu et al., 2011)

5.2 Anisotropic elastic metamaterials and boundary effective medium theory

The rubber-coated water cylinder embedded in foam provides the possibility of realizing double negative shear bands. The isotropic scatterers and the hexagonal lattice structure result in a simple isotropic effective medium description of the metamaterial, which makes the design of the elastic metamaterial easier. If there is no restriction on the symmetry properties of the scatterer, there would be much more choices at the cost of many more complicated microstructures of the scatterers.

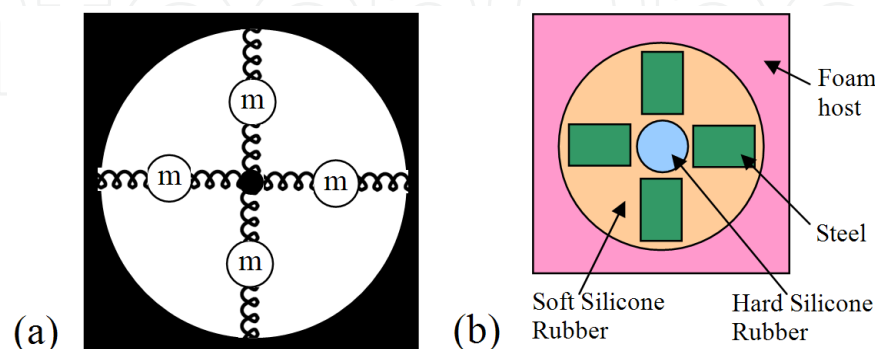


Fig. 10. A schematic figure of the physical model and the practical design. (Lai et al., 2011)

Since Fig. 5(b) exhibits a four-fold symmetry of a quadrupolar resonance, inserting heavier objects into the rubber in a way that is in accordance with the field pattern would help enhance the resonance. Figure 10(a) is a schematic figure of the physical model of the unit cell, which shows four masses connected to their center and the host (Lai et al., 2011). Such a structure is favorable of enhancing the dipolar resonance by the collective motion of the four masses, and the quadrupolar and monopolar resonances by relative motions of the masses. A practical realization of the model is illustrated in Fig. 10(b). The scatterers are composed of four steel rods surrounding a hard silicone rubber cylinder embedded in a soft silicone rubber cylinder. The matrix material is still foam. The lattice structure is a square with lattice constant of 10cm ; the radii of the soft and hard silicone rubber rods are 4cm and 1cm , respectively; the rectangular steel rods are $1.6\text{cm} \times 2.4\text{cm}$ in size, located at a distance of 2.4cm from the center. The material parameters for the foam and soft silicone rubber remain the same as the ones used in the design of rubber-coated water cylinder. The hard silicone rubber and the steel have parameters of: $\rho = 1.415 \times 10^3 \text{ kg/m}^3$, $\lambda = 1.27 \times 10^9 \text{ N/m}^2$ and $\mu = 1.78 \times 10^6 \text{ N/m}^2$ for hard silicone rubber and $\rho = 7.9 \times 10^3 \text{ kg/m}^3$, $\lambda = 1.11 \times 10^{11} \text{ N/m}^2$ and $\mu = 8.28 \times 10^{10} \text{ N/m}^2$ for steel. The four rectangular steel rods serve as the four masses and the soft silicone rubber rods serve as the springs. The insertion of the hard silicone rubber is for the purpose of adjusting the spring constants between the masses.

The band structure of such metamaterial was calculated by using a finite element solver (COMSOL Multiphysics) and is shown in Fig. 11(a). There are two negative bands (red and blue dots), where the lower one (red dots) has a bandwidth about 18 Hz and the higher one (blue dots) has band widths of 18 Hz and 10 Hz along ΓM and ΓX direction respectively. These two bands are separated by a small complete gap (178 Hz~198 Hz). The two eigenstates in the lower and upper negative bands at the Γ point are plotted in Figs. 11(b)

and 11(c), respectively. The eigenstate in Fig. 11(b) is clearly a quadrupolar resonance, whereas the eigenstate in Fig. 11(c) is a monopolar resonance.

The negative bands can also be understood from an effective medium point of view. Since the scatterer involves a four-fold symmetry, the previously derived formula based on MST for isotropic inclusions does not apply and an EMT based on boundary integration is

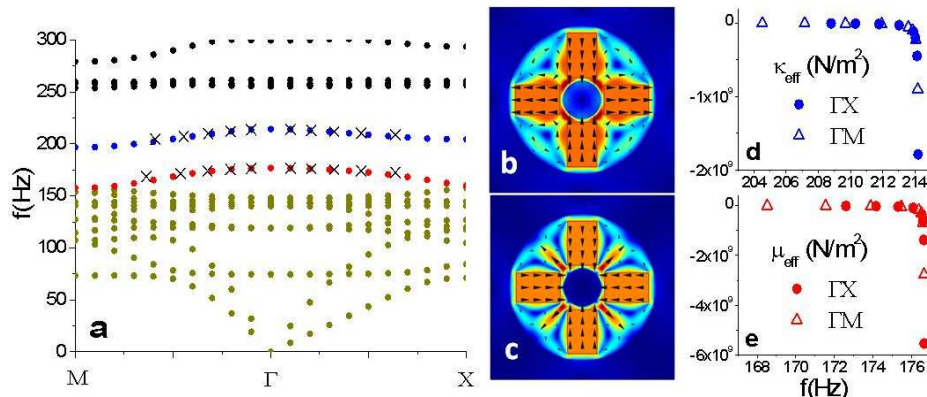


Fig. 11. (a) Band structure of the multi-mass metamaterial. (b) and (c) Displacement field of eigenstates. The color represents the amplitude of displacement (blue/red for small/large values) and the arrows show the displacement vectors directly. (d) and (e) effective medium parameters calculated by a boundary EMT. (Lai et al., 2011)

developed. Though the scatterer is anisotropic, the dispersions and the associated modes can still be obtained from Christoffel's equation, i.e., Eqs. (35) and (36), with three independent effective moduli, C_{11} , C_{12} and C_{44} , and a mass density, ρ . The task is to determine the values of these parameters. The mass density is determined by Newton's law, $\rho^e = -F_x^e / \omega^2 u_x^e a^2$, where both the effective force F_x^e on the unit cell and its effective displacement u_x^e may be obtained from surface integration of the stresses (along the x direction) and the displacements over the unit cell, i.e.,

$$F_x^e = \int T_{xx} dy \Big|_{x=a} - \int T_{xx} dy \Big|_{x=0} + \int T_{xy} dx \Big|_{y=a} - \int T_{xy} dx \Big|_{y=0} \quad (37)$$

and

$$u_x^e = \frac{\int u_x dy \Big|_{x=0} + \int u_x dy \Big|_{x=a}}{2a} \quad (38)$$

The stresses and displacements can be obtained from the COMSOL calculation. Similarly, the effective moduli are evaluated from the effective stress and strain relations: $T_{xx}^e = C_{11}^e S_{xx}^e + C_{12}^e S_{yy}^e$, $T_{yy}^e = C_{12}^e S_{xx}^e + C_{11}^e S_{yy}^e$, and $T_{xy}^e = 2C_{44}^e S_{xy}^e$, where both the effective stresses and the effective strains are evaluated on the unit cell boundary as follows:

$$T_{xx}^e = \frac{\int T_{xx} dy \Big|_{x=0} + \int T_{xx} dy \Big|_{x=a}}{2a}; T_{yy}^e = \frac{\int T_{yy} dy \Big|_{y=0} + \int T_{yy} dy \Big|_{y=a}}{2a};$$

$$T_{xy}^e = \frac{\int T_{xy} dx|_{y=0} + \int T_{xy} dx|_{y=a}}{2a}; T_{yx}^e = \frac{\int T_{xy} dy|_{x=0} + \int T_{xy} dy|_{x=a}}{2a} \quad (39)$$

and

$$S_{xx}^e = \frac{\int u_x dy|_{x=a} - \int u_x dy|_{x=0}}{a^2}; S_{yy}^e = \frac{\int u_y dy|_{y=a} - \int u_y dy|_{y=0}}{a^2} \quad (40)$$

$$S_{xy}^e = \frac{\int u_x dx|_{y=a} - \int u_x dx|_{y=0} + \int u_y dy|_{x=a} - \int u_y dy|_{x=0}}{2a^2}$$

Though the above equations are presented for calculations along the ΓX direction, the corresponding formula for ΓM direction can be similarly transcribed. Due to the obvious link between the bulk (shear) modulus and monopolar (quadrupolar) resonance, it is more convenient to introduce $\kappa_{\text{eff}} = (C_{11} + C_{12})/2$ and $\mu_{\text{eff}} = (C_{11} - C_{12})/2$ as effective elastic bulk modulus and shear modulus. The results for κ_{eff} and μ_{eff} evaluated from the relevant eigenstates are plotted in Figs. 11(d) and 11(e). In the lower negative band, κ_{eff} is positive and finite, while μ_{eff} is negative and diverges at the Γ point, which is in accordance with the quadrupolar resonance. In the higher negative band, μ_{eff} is positive and finite, while κ_{eff} is negative and diverges at the Γ point, which is induced by the monopolar resonance.

Knowing the effective moduli, the corresponding dispersion relations can be calculated by using Christoffel's equation. Along the ΓX direction, compressional wave and shear wave velocities are given by $\sqrt{C_{11}/\rho}$ and $\sqrt{C_{44}/\rho}$, respectively; whereas along the ΓM direction the compressional and shear wave velocities are $\sqrt{(C_{11} + C_{12} + 2C_{44})/(2\rho)}$ and $\sqrt{(C_{11} - C_{12})/(2\rho)}$. The effective medium results show that the lower negative band supports a longitudinal (transverse) wave along ΓX (ΓM) direction, whereas the upper negative band only allows longitudinal wave in both ΓX and ΓM directions. The corresponding results obtained from the EMT are also plotted in Fig. 11(a) by crosses. Excellent agreements between the finite element results and the EMT prediction are found.

6. Some intriguing properties of elastic metamaterials

Like their EM and acoustic counterparts, elastic metamaterials have shown many intriguing wave transport properties. For example, the total mode conversion and the super-anisotropy are two of them. The total mode conversion can completely convert the incident transverse (longitudinal) wave into a refracted longitudinal (transverse) wave. It is an analogue of the Brewster angle in the EM case (for example, Jackson, 1999), but in a much more stringent and complex manner. It only occurs on the interface between a normal solid and an elastic metamaterial with negative refractive index (Wu et al. 2011). The super-anisotropic behavior has been demonstrated in Section 5.2. Also shown there is the property of sustaining only a longitudinal wave at certain frequencies, which is so-called "fluid-like" solids, blurring the distinction between solids and fluids (Lai et al., 2011).

7. Conclusion

In this chapter, the effective medium properties of 2D elastic metamaterials have been reviewed. Unlike EM or acoustic metamaterials, the elastic metamaterial is in general anisotropic unless the lattice structure is a hexagon with isotropic scatterers. For the isotropic elastic metamaterial, the EMT may be derived from CPA. For the anisotropic metamaterial, the EMT may be obtained from the MST in conjunction with Christoffel's equation, or from the integration of eigenfields on the boundaries. EMT could greatly facilitate the design of new elastic metamaterials, such as rubber-coated water cylinder embedded in foam which gives rise to large negative bands for shear waves and a multi-mass locally resonant structure which results in both negative bands for longitudinal waves and super-anisotropic negative bands.

Elastic metamaterial opens a new research area. The experimental realization would be much more challenging and exciting. The generalization of EMT as well as the symmetry property to more complex lattice structures, such as rectangular lattices, would also be of interest as it will introduce even stronger anisotropy. Meanwhile, finding an EMT that can also treat the rotational modes is a challenging task. Such modes are normally excited at lower frequencies and form flat bands in the band structures.

8. Acknowledgments

The relevant work was supported by Hong Kong RGC Grant No. 605008, and start-up packages from KAUST and Soochow University.

9. References

- Abramowitz, M. & Stegun, I. (Eds.). (1972). *Handbook of Mathematical Functions: with Formulas, Graphs, and Mathematical Tables*, Dover, ISBN 0486612724, New York
- Andrea, A. (2011). First-Principle Homogenization Theory for Periodic Metamaterials, *Physical Review B*, Vol.84, No.7, (Aug 2011), pp. 075153, ISSN 1098-0121
- Andryieuski, A.; Malureanu, R. & Lavrinenko, A. (2009). Wave Propagation Retrieval Method for Metamaterials: Unambiguous Restoration of Effective Parameters, *Physical Review B*, Vol.80, No.19, (Nov 2009), pp.193101, ISSN 1098-0121
- Baker-Jarvis, J.; Vanzura, E. & Kissick, W. (1990). Improved Technique for Determining Complex Permittivity with the Transmission/Reflection Method, *IEEE Transactions on microwave theory and techniques*, Vol.38, No.8, (August 1990), pp. 1096-1103, ISSN 0018-9480
- Berryman, J. (1980). Long-wavelength Propagation in Composite Elastic Media. 1. Spherical Inclusions, *Journal of the Acoustical Society of America*, Vol.68, No.6, pp. 1809-1819, ISSN 0001-4966
- Chern, R. & Chen, Y. (2009). Effective Parameters for Photonic Crystals with Large Dielectric Contrast, *Physical Review B*, Vol.80, No.7, (August 2009), pp. 075118, ISSN 0163-1829
- Chen, H.; Chan, C. & Sheng, P. (2010). Transformation Optics and Metamaterials, *Nature Materials*, Vol.9, No.5, (May 2010), pp.387-396, ISSN 1476-1122

- Chen, H.; Fung, K.; Ma, H. & Chan, C. (2008). Polarization Gaps and Negative Group Velocity in Chiral Phononic Crystals, *Physical Review B*, Vol.77, No.22, (June 2008), pp. 224304, ISSN 0163-1829
- Chin, S.; Nicorovici, N. & McPhedran, R. (1994). Green's Function and Lattice Sums for Electromagnetic Scattering by a Square Array of Cylinders. *Physical Review E*, Vol.49, No.5, (May 1994), pp. 4590-4602, ISSN 1063-651X
- Chui, S. & Hu, L. (2002). Theoretical Investigation on the Possibility of Preparing Left-Handed Materials in Metallic Magnetic Granular Composites, *Physical Review B*, Vol.65, No.14, (March 2002), pp. 144407, ISSN 0163-1829
- Chui, S. & Lin, Z. (2008). Long-Wavelength Behavior of Two-Dimensional Photonic Crystals. *Physical Review E*, Vol.78, No.6, (December 2008), pp.065601 ISSN 1539-3755
- Ding, Y.; Liu, Z.; Qiu, C. & Shi, J. (2007). Metamaterial with Simultaneously Negative Bulk Modulus and Mass Density, *Physical Review Letters*, Vol.99, No.9, (August 2007), pp. 093904, ISSN 0031-9007
- Fang, N.; Xi, D.; Xu, J.; Ambati, M.; Srituravanich, W.; Sun, C. & Zhang, X. (2006). Ultrasonic Metamaterials with Negative Modulus, *Nature Materials*, Vol.5, No.6, (June 2006), pp. 452-456, ISSN 1476-1122
- Grbic, A. & Eleftheriades, G. (2004). Overcoming the Diffraction Limit with a Planar Left-Handed Transmission-Line Lens, *Physical Review Letters*, Vol.92, No.11, (March 2004), pp. 117403 ISSN 0031-9007
- Hashin, Z. & Shtrikman, S. (1963). A Variational Approach to The Theory of The Elastic Behaviour of Multiphase Materials, *Journal of the Mechanics and Physics of Solids*, Vol.11, No.2, pp. 127-140, ISSN: 0022-5096
- Hu, X.; Chan, C.; Zi, J.; Li, M. & Ho, K. (2006). Diamagnetic Response of Metallic Photonic Crystals at Infrared and Visible Frequencies, *Physical Review Letters*, Vol.96, No.22, (June 2006), pp. 223901, ISSN 0031-9007
- Jackson, J.; (1999). *Classical Electrodynamics* (Third edition), John Wiley, ISBN 0-471-30932-X, New York
- Jin, J.; Liu, S.; Lin, Z. & Chui, S. (2009). Effective-Medium Theory for Anisotropic Magnetic Metamaterials, *Physical Review B*, Vol.80, No.11, (September 2009), pp.115101, ISSN 0163-1829
- Kafesaki, M. & Economou, E. (1999). Multiple-scattering Theory for Three-dimensional Periodic Acoustic Composites, *Physical Review B*, Vol.60, No.17, (November 1999), pp. 11993-12001, ISSN 0163-1829
- Kafesaki, M.; Penciu, R. & Economou, E. (2000). Air Bubbles in Water: A Strongly Multiple Scattering Medium for Acoustic Waves, *Physical Review Letters*, Vol.84, No.26, (June 2000), pp. 6050-6053, ISSN 0031-9007
- Krokhin, A.; Arriaga, J. & Gumen, L. (2003). Speed of Sound in Periodic Elastic Composites, *Physical Review Letters*, Vol.91, No.26, (December 2003), pp. 264302, ISSN 0031-9007
- Lai, Y.; Wu, Y.; Sheng, P. & Zhang, Z. (2011). Hybrid Elastic Solids, *Nature Materials*, Vol.10, No.8, (August 2011), pp. 620-624, ISSN 1476-1122

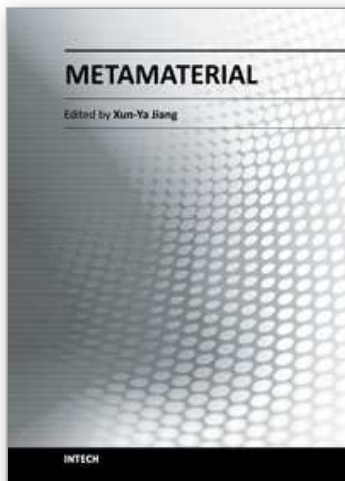
- Lamb, W.; Wood, D. & Ashcroft, N. (1980). Long-Wavelength Electromagnetic Propagation in Heterogeneous Media, *Physical Review B*, Vol.21, No.6, (March 1980), pp.2248-2266, ISSN 0163-1829
- Landau, L. & Lifshitz, E. (1986). *Theory of Elasticity* (Third edition), Butterworth-Heinemann, ISBN 0 7506 2633 X, Oxford
- Lee, S.; Park, C.; Seo, Y.; Wang, Z. & Kim, C. (2010). Composite Acoustic Medium with Simultaneously Negative Density and Modulus, *Physical Review Letters*, Vol.104, No.5, (February 2010), pp. 054301, ISSN 0031-9007
- Leonhardt, U. (2006). Optical Conformal Mapping, *Science*, Vol.312, No.5781, (June 2006), pp.1777-1780, ISSN 0036-8075
- Lezec, H.; Dionne, J. & Atwater, H. (2007). Negative Refraction at Visible Frequencies, *Science*, Vol.361, No.5823, (April 2007), pp. 430-432, ISSN 0036-8075
- Li, J. & Chan C. (2004). Double-negative Acoustic Metamaterial, *Physical Review E*, Vol.70, No.5,(November 2004),pp.055602, ISSN 1063-651X
- Liu, Z.; Chan, C.; Sheng, P.; Goertzen, A. & Page, J. (2000). Elastic Wave Scattering by Periodic Structures of Spherical Objects: Theory and Experiment, *Physical Review B*, Vol.62, No.4, (July 2000), pp. 2446-2457, ISSN 1098-0121
- Liu, Z.; Zhang, X.; Mao, Y.; Zhu, Y.; Yang, Z.; Chan, C. & Sheng, P. (2000) Locally Resonant Sonic Materials, *Science*, Vol.289, No.5485, (September 2000), pp. 1734-1736, ISSN 0036-8075
- Lu, M.; Feng, L. & Chen, Y. (2009). Phononic Crystals and Acoustic Metamaterials, *Materials Today*, Vol.12, No.12, (December 2009), pp. 34-42, ISSN: 1369-7021
- Mei, J.; Liu, Z.; Wen, W. & Sheng, P. (2006). Effective Mass Density of Fluid-solid Composites, *Physical Review Letters*, Vol.96, No.2, (January 2006), pp. 024301, ISSN 0031-9007
- Mei, J.; Liu, Z.; Shi, J. & Tian, D. (2003). Theory for Elastic Wave Scattering by a Two-Dimensional Periodical Array of Cylinders: An Ideal Approach for Band-Structure Calculations, *Physical Review B*, Vol.67, No.24, (June 2003), pp. 245107, ISSN 1098-0121
- Milton, G. & Willis, J. (2007). On Modification of Newton's Second Law and Linear Continuum Elastodynamics, *Proceedings of the Royal Society A-Mathematical Physical and Engineering Sciences*, Vol.463, No.2079, (March 2007), pp.855-880, ISSN1364-5021
- Ni, Q. & Cheng, J. (2005). Anisotropy of Effective Velocity for Elastic Wave Propagation in Two-Dimensional Phononic Crystals at Low Frequencies, *Physical Review B*, Vol.72, No.1, (July 2005), pp. 014305, ISSN 0163-1829
- Pendry, J. (2000). Negative Refraction Makes a Perfect Lens, *Physical Review Letters*, Vol.85, No.18, (October 2000), pp. 3966-3969, ISSN 0031-9007
- Pendry, J.; Holden, A.; Robbins, D. & Stewart, W. (1999). Magnetism from Conductors and Enhanced Nonlinear Phenomena, *IEEE Transactions on Microwave Theory and Techniques*, Vol.47, No.11, (November 1999), pp. 2075-2084, ISSN 0018-9480
- Pendry, J.; Holden, A.; Stewart, W. & Youngs, I. (1996). Extremely Low Frequency Plasmons in Metallic Mesostructures, *Physical Review Letters*, Vol.76, No.25, (June 1996), pp. 4773-4776, ISSN 0031-9007

- Pendry, J.; Schurig, D. & Smith, D. (2006). Controlling Electromagnetic Fields, *Science*, Vol.312, No. 5781, (June 2006) pp.1780-1782, ISSN 0036-8075
- Pendry, J. & Smith, D. (2006). The Quest for the Superlens, *Scientific America*, Vol.295, No.1, (July 2006), pp. 60-67, ISSN 0036-8733
- Royer, D. & Dieulesaint, E. (1999). *Elastic Waves in Solids I: Free and Guided Propagation* (First edition), Springer, ISBN 3540659323, Berlin
- Sheng, P. (2006). *Introduction to Wave Scattering, Localization, and Mesoscopic Phenomena* (Second edition), Springer, ISBN-10 3-540-29155-5, Berlin Heidelberg
- Smith, D. & Pendry, J. (2006). Homogenization of Metamaterials by Field Averaging (Invited Paper), *Journal of the Optical Society of America B-Optical Physics*, Vol.23, No.2 (March 2006), pp.391-403, ISSN 0740-3224
- Smith, D.; Schultz, S.; Markos, P. & Soukoulis, C. (2002). Determination of Effective Permittivity and Permeability of Metamaterials from Reflection and Transmission Coefficients, *Physical Review B*, Vol.65, No.19, (May 2002), pp.195104, ISSN 1098-012
- Sun, S.; Shui, S. & Zhou, L. (2009). Effective-Medium Properties of Metamaterials: A Quasimode Theory, *Physical Review E*, Vol.79, No.6, (June 2009), pp.066604, ISSN 1063-651X
- Torquato, S. (1991). Random Heterogeneous Media: Microstructure and Improved Bounds on Effective Properties, *Applied Mechanics Reviews*, Vol.44, No.2, (February 1991) pp. 37-76, ISSN 0003-6900
- Torrent, D.; Hakansson, A.; Cervera, F. & Sanchez-Dehesa, J. (2006). Homogenization of Two-Dimensional Clusters of Rigid Rods in Air, *Physical Review Letters*, Vol.96, No.20, (May 2006), pp. 204302, ISSN 0031-9007
- Veselago, V. (1968). The Electrodynamics of Substances with Simultaneously Negative Values of ϵ and μ , *Soviet Physics Uspekhi*, Vol.10, No.4, pp. 509
- Wu, Y.; Li, J.; Zhang, Z. & Chan C. (2006). Effective Medium Theory for Magnetodielectric Composites: Beyond the Long-Wavelength Limit, *Physical Review B*, Vol.74, No.8, (August 2006), pp.085111, ISSN 1098-0121
- Wu, Y.; Lai, Y. & Zhang, Z. (2007). Effective Medium Theory for Elastic Metamaterials in Two Dimensions. *Physical Review B*, Vol.76, No.20, (November 2007), pp.025313, ISSN 1098-0121
- Wu, Y.; Lai, Y. & Zhang, Z. (2011). Elastic Metamaterials with Simultaneously Negative Effective Shear Modulus and Mass Density, *Physical Review Letters*, Vol.107, No.10, (September 2011), pp. 105506, ISSN 0031-9007
- Wu, Y. & Zhang, Z. (2009). Dispersion Relations and Their Symmetry Properties of Electromagnetic and Elastic Metamaterials in Two Dimensions, *Physical Review B*, Vol.79, No.19, (May 2009), pp.195111, ISSN 1098-0121
- Yang, Z.; Mei, J.; Yang, M.; Chan, N. & Sheng, P. (2008) Membrane-Type Acoustic Metamaterial with Negative Dynamic Mass, *Physical Review Letters*, Vol.101, No.20, (November 2008), pp.204301, ISSN 0031-9007
- Zhang, S.; Xia, C. & Fang, N. (2011). Broadband Acoustic Cloak for Ultrasound Waves, *Physical Review Letters*, Vol.106, No.2, (January 2011), pp. 024301, ISSN 0031-9007

- Zhang, S.; Yin, L. & Fang, N. (2009). Focusing Ultrasound with an Acoustic Metamaterial Network, *Physical Review Letters*, Vol.102, No.19, (May 2009), pp. 194301, ISSN 0031-9007
- Zhou, X. & Hu, G. (2009). Analytic Model of Elastic Metamaterials with Local Resonances, *Physical Review B*, Vol.75, No.19, (May 2009), pp.195109, ISSN 1098-0121

IntechOpen

IntechOpen



Metamaterial

Edited by Dr. Xun-Ya Jiang

ISBN 978-953-51-0591-6

Hard cover, 620 pages

Publisher InTech

Published online 16, May, 2012

Published in print edition May, 2012

In-depth analysis of the theory, properties and description of the most potential technological applications of metamaterials for the realization of novel devices such as subwavelength lenses, invisibility cloaks, dipole and reflector antennas, high frequency telecommunications, new designs of bandpass filters, absorbers and concentrators of EM waves etc. In order to create a new devices it is necessary to know the main electrodynamical characteristics of metamaterial structures on the basis of which the device is supposed to be created. The electromagnetic wave scattering surfaces built with metamaterials are primarily based on the ability of metamaterials to control the surrounded electromagnetic fields by varying their permeability and permittivity characteristics. The book covers some solutions for microwave wavelength scales as well as exploitation of nanoscale EM wavelength such as visible specter using recent advances of nanotechnology, for instance in the field of nanowires, nanopolymers, carbon nanotubes and graphene. Metamaterial is suitable for scholars from extremely large scientific domain and therefore given to engineers, scientists, graduates and other interested professionals from photonics to nanoscience and from material science to antenna engineering as a comprehensive reference on this artificial materials of tomorrow.

How to reference

In order to correctly reference this scholarly work, feel free to copy and paste the following:

Ying Wu, Yun Lai and Zhao-Qing Zhang (2012). Effective Medium Theories and Symmetry Properties of Elastic Metamaterials, Metamaterial, Dr. Xun-Ya Jiang (Ed.), ISBN: 978-953-51-0591-6, InTech, Available from: <http://www.intechopen.com/books/metamaterial/effective-medium-theories-and-symmetry-properties-of-elastic-metamaterials>

INTECH
open science | open minds

InTech Europe

University Campus STeP Ri
Slavka Krautzeka 83/A
51000 Rijeka, Croatia
Phone: +385 (51) 770 447
Fax: +385 (51) 686 166
www.intechopen.com

InTech China

Unit 405, Office Block, Hotel Equatorial Shanghai
No.65, Yan An Road (West), Shanghai, 200040, China
中国上海市延安西路65号上海国际贵都大饭店办公楼405单元
Phone: +86-21-62489820
Fax: +86-21-62489821

© 2012 The Author(s). Licensee IntechOpen. This is an open access article distributed under the terms of the [Creative Commons Attribution 3.0 License](#), which permits unrestricted use, distribution, and reproduction in any medium, provided the original work is properly cited.

IntechOpen

IntechOpen